Research Article

Muhammad Nasir Amin*, Ahmed A. Alawi Al-Naghi, Roz-Ud-Din Nassar, Omar Algassem, Suleman Ayub Khan*, and Ahmed Farouk Deifalla*

Investigating the rheological characteristics of alkali-activated concrete using contemporary artificial intelligence approaches

https://doi.org/10.1515/rams-2024-0006 received December 06, 2023; accepted March 04, 2024

Abstract: Using artificial intelligence-based tools, this research aims to establish a direct correlation between the alkali-activated concrete (AAC) mix design factors and their performances. More specifically, the machine learning system was fed new property data obtained from AAC mixes used in laboratory experiments. The rheological parameters (yield stress [static/dynamic] and plastic viscosity) of AAC were predicted using the multilayer perceptron neural network (MLPNN) and bagging ensemble (BE) models. In addition, the R^2 values, k-fold analyses, statistical checks, and the dissimilarity between the experimental and predicted compressive strength were employed to assess the performance of the created models. Also, the SHapley additive exPlanation (SHAP) approach was used for examining the relevance of influencing parameters. The BE approach was found to be significantly accurate in all prediction models, with R^2 greater than 0.90, and MLPNN models were found to be moderately precise, with R^2 slightly below 0.90. However, the error assessment through statistical checks and k-fold analysis also validated the higher precision of BE models over the MLPNN models. Building models that can calculate rheological properties of AAC for

different values of input parameters could save a lot of time and money compared to doing the tests in a laboratory. In order to ascertain the required amounts of raw materials of AAC, investigators, as well as businesses, may find the SHAP study helpful.

Keywords: rheological properties, alkali-activated concrete, multilayer perceptron neural networks

1 Introduction

Due to its numerous benefits in relation to approachability, budget, and other factors, concrete has become the most popular building material [1]. However, rising urbanization in recent years has led to a rise in the necessity for concrete, has a significant impact on the planet, and has grown into a major problem that worries people all across the world. Ordinary portland cement (OPC) is the most widely used binder in concrete, although its manufacturing requires significant amounts of energy. OPC clinker manufacturing has been linked to 5–8% of worldwide CO₂ emissions [2], putting significant emphasis on achieving carbon neutrality by 2050. As a low-carbon binder, alkaliactivated material (AAM) has the potential to substitute OPC materials in concrete. OPC materials undergo an alkali-activation process rather than hydration as a result of the persistent dissolution of alumino-silicate precursors in alkaline environments [3]. An important first step in reassembling highly organized structures is to use polymerizations to connect the dissolved Al and Si tetrahedrons to each other as the backbone [4–6], and then the alkali/ alkali-earth cations are added. A high calcium content in the precursors has a significant impact on the microstructure of the reaction products, according to the research [7].

However, in practice, precursors, particularly those derived from different types of waste, lack sufficient reactivity. The use of alkaline activators to speed up dissolution brings additional complexity to the AAM scheme through

^{*} Corresponding author: Muhammad Nasir Amin, Department of Civil and Environmental Engineering, College of Engineering, King Faisal University, Al-Ahsa 31982, Saudi Arabia, e-mail: mgadir@kfu.edu.sa

^{*} Corresponding author: Suleman Ayub Khan, Department of Civil Engineering, COMSATS University Islamabad, Abbottabad 22060, Pakistan, e-mail: sulemanayub@cuiatd.edu.pk

^{*} Corresponding author: Ahmed Farouk Deifalla, Department of Structural Engineering and Construction Management, Future University in Egypt, New Cairo City 11835, Egypt, e-mail: ahmed.deifalla@fue.edu.eg Ahmed A. Alawi Al-Naghi, Omar Algassem: Civil Engineering Department, University of Ha'il, Ha'il 55476, Saudi Arabia Roz-Ud-Din Nassar: Department of Civil and Infrastructure Engineering, American University of Ras Al Khaimah, Ras Al-Khaimah, United Arab Emirates

the introduction of novel interactions [8]. Many different types of precursors and alkaline elements can be used in AAMs to recycle industrial by-products, which is their main purpose. With so many different building blocks to pick from, it is easy to imagine all sorts of unique permutations. To reliably and predictably produce appropriate AAM mix designs, however, additional data regarding the reaction mechanisms are required, and creating a normal design code is challenging due to differences in material characteristics [9]. Although there are many different alkali-activated concrete (AAC) products on the market, their use in construction is still restricted to a handful of demonstration buildings because of immature design rules [10]. Therefore, these methods may significantly increase AAC production pre-design time.

An artificial intelligence strategy for encapsulating the characteristics of heterogeneous and intricate systems has been established with the advent of ML algorithms [11–15]. Gradient boosting, artificial neural networks (ANNs), support vector machines (SVMs), random forests, and so on have all been used to effectively predict the performance of OPC concretes in the past [16-23]. The emergence of ML algorithms has given a handy way to forecast performance from experimental data, which is especially helpful given the diversity and complexity of AACs [24-27]. It is noted that the majority of the AAC models used presently prioritize mechanical attributes. Ramagiri et al. demonstrated this by combining the AAC strength prediction outcomes of five RA-F models with different topologies [28]. In order to find the compressive strength (CS) of 162 AAC mixes that contained fly ash, Toufigh and Jafari created an estimating approach [29]. By utilizing extreme learning machine (ELM), SVM, and ANN techniques, Peng and Unluer were able to forecast the CS of F-ash-based AAC with a 20% accuracy rate [30]. In order to develop models for forecasting the CS and initial slump flow of AAC, Gomaa et al. performed a large number of trials [31]. On the other hand, information on AAC's processing capacity and rheological characteristics is severely lacking in both data and models.

This study included findings from 52 AAC mix laboratory tests (145 data of rheological properties). The static/dynamic yield stress (SYS/DYS) and plastic viscosity (PV) of AAC were predicted using multilayer perceptron neural network (MLPNN) models and bagging ensemble (BE) models depending on the seven parameters that were input: precursor content (PC), aggregate, sodium hydroxide (NaOH), silica/sodium oxide ratio (SiO₂/Na₂O), blast furnace slag (BFS), water, and testing age (TA). The models were validated with statistical tests and k-fold analysis, and the influence of the variables on the prediction was examined using SHapley Additive exPlanations (SHAP) analysis. SHAP

analysis of the rheological features of ACC with the specified input parameters has been the primary focus of this work. The important parameters that may play a role in the subsequent ACC mix design computation are revealed by SHAP analysis. Moreover, new attributes acquired can be used to augment the existing AAC database, while the built regression models may offer direction on AAC mix design. ML models for AAC property prediction are faster, cheaper, and more accurate than conventional testing methods. They optimize AAC formulations, decrease experimental testing, and improve AAC structure design and quality control compared to existing methods.

2 Study methods

2.1 Acquiring and analyzing data

Utilizing a set of data of 145 points from the literature [21] with MLPNN and BE models, this study aimed to anticipate the static yield stress (SYS), dynamic yield stress (DYS), and PV of AAC. The SYS, DYS, and PV of AAC were predicted in this work using seven input factors. In order to gather and arrange the data, data preparation was employed. As part of the well-known process of knowledge discovery from data, one method for overcoming a significant impediment is to prepare data for data mining. The objective of the data preparation process is to simplify the data by removing noise and other information that is not crucial to the analysis. It has also been hypothesized by specialists from a wide variety of fields that the proportion of data points to inputs is an essential factor in determining how well the proposed model will function [32,33]. It is necessary for the optimal model to have a ratio that is more than five, which is the number of datasets divided by the number of input parameters. This ratio enables the testing of data points to determine the connection between the variables that have been chosen [33]. In order to estimate the SYS, DYS, and PV of ACC, the current study makes use of seven inputs. The ratio that is obtained as a consequence, which is 20.71, is satisfactory to the requirements that were established by the researchers. In order to conduct the analysis of the model, regression and error-distribution methods were utilized. Specifically, descriptive statistics on these data are presented in Table 1, which displays the findings of those statistics. The validity approach has also been utilized in order to assess the accuracy of the models that were utilized. A clear illustration of the statistical distribution of

Table 1: Statistics-based variable descriptions [34]

Descriptive statistics	PC (kg·m ^{−3})	BFS (%)	NaOH (kg·m ⁻³)	SiO ₂ / Na ₂ O	Water (kg·m ^{−3})	Aggregate (kg·m ⁻³)	TA (min)	SYS (Pa)	DYS (Pa)	PV (Pa·s)
Mean	378.30	92.07	14.84	0.50	175.57	1795.34	28.59	1242.50	259.32	122.63
Standard error	2.86	1.21	0.35	0.02	0.80	4.55	1.83	100.26	19.40	6.37
Median	369.00	100.00	14.40	0.50	176.00	1815.00	20.00	773.00	168.82	99.29
Mode	369.00	100.00	14.17	0.50	176.00	1815.00	5.00	501.87	106.68	55.20
Standard	34.41	14.58	4.26	0.27	9.65	54.77	21.99	1207.32	233.59	76.73
deviation										
Sample variance	1184.34	212.70	18.11	0.08	93.15	3000.01	483.58	1457629.00	54562.82	5887.06
Kurtosis	4.04	1.82	0.12	0.60	1.00	6.09	-1.28	9.04	2.21	1.68
Skewness	2.19	-1.75	0.04	0.43	-0.53	-2.60	0.37	2.47	1.64	1.57
Range	167.50	50.00	19.87	1.25	44.00	312.00	60.00	8328.81	1040.25	335.60
Minimum	320.00	50.00	5.29	0.00	151.00	1574.00	5.00	114.12	6.25	37.28
Maximum	487.50	100.00	25.16	1.25	195.00	1886.00	65.00	8442.93	1046.50	372.88
Sum	54853.00	13350.00	2151.53	72.25	25457.00	260325.00	4145.00	180161.89	37601.44	17781.09
Count	145.00	145.00	145.00	145.00	145.00	145.00	145.00	145.00	145.00	145.00

each variable may be found in the violin plots presented in Figure 1. For the purpose of providing an explanation for the overall frequency distribution of a data collection, the distributions of the individual input variables can be utilized. Developing a relative frequency dispersal, which illustrates the occurrence with which parameter values appear, is one method that may be utilized to investigate the data.

2.2 Machine learning modeling

The properties of AAC's rheology were tested in the lab. The processes required seven inputs and returned three outcomes: SYS, DYS, and PV. The goals of the study were attained by the use of Python and Spyder (5.1.5) scripts run through Anaconda Navigator. The SYS, DYS, and PV of AAC were predicted using both standalone ML methods (such as MLPNN) and ensemble ML methods (like BE). Common practice involves analyzing outputs in the context of input features using ML algorithms. While 70% of the data was utilized to train machine learning models, only 30% was used for actual testing. The data split is essential to evaluating machine learning models since it trains the model to learn patterns on most of the data and then tests its generalization ability on an independent sample. This split helps evaluate the model's predicting abilities on unknown data without over-fitting to the training set. Other scholars have adopted similar splitting ratios in various studies [35,36]. R^2 of the expected result demonstrated the efficiency of the model used. A low R^2 value implies a big difference between the predicted and observed values,

while a high value suggests a high degree of resemblance [37]. The model's accuracy was confirmed by employing a diversity of methods, including statistical tests, error assessments, and k-fold methodologies. Schematically represented in Figure 2 is an example of event modeling.

2.2.1 MI PNN model

Among the many ML models, the ANN is among the most powerful. Ecological and hydrological engineering have made extensive use of it to address non-linear issues. The MLPNN is now the most utilized ANN model. The MLPNN approach has a three-layer structure consisting of input, hidden, and output layers. Tansig, purelin, and Logsig are the top three most usual triggering functions. Activations, weights, and biased coefficients for the output and hidden layers demand a lot of consideration. All of the model's parameters, or weights, are set to their final values as it is being trained. Applying the k-fold approach ensures the optimal structure is achieved. To construct the most effective ANN model, the three hidden layers (i.e., 7, 5, and 4) that included the most number of neurons were utilized [38]. In order to construct the system, the frontward-pass input is lead, the weight is utilized, and a rough approximation of the technique's output is formed. These three processes constitute the creation of the system. The results of the calculations are then compared against the inputs used to generate them. The model accounts for the inputs while making predictions. Different outcomes can be attained by employing various loss functions. It is possible to derive the partial derivatives of the cost function that are specific to each operational factor by employing

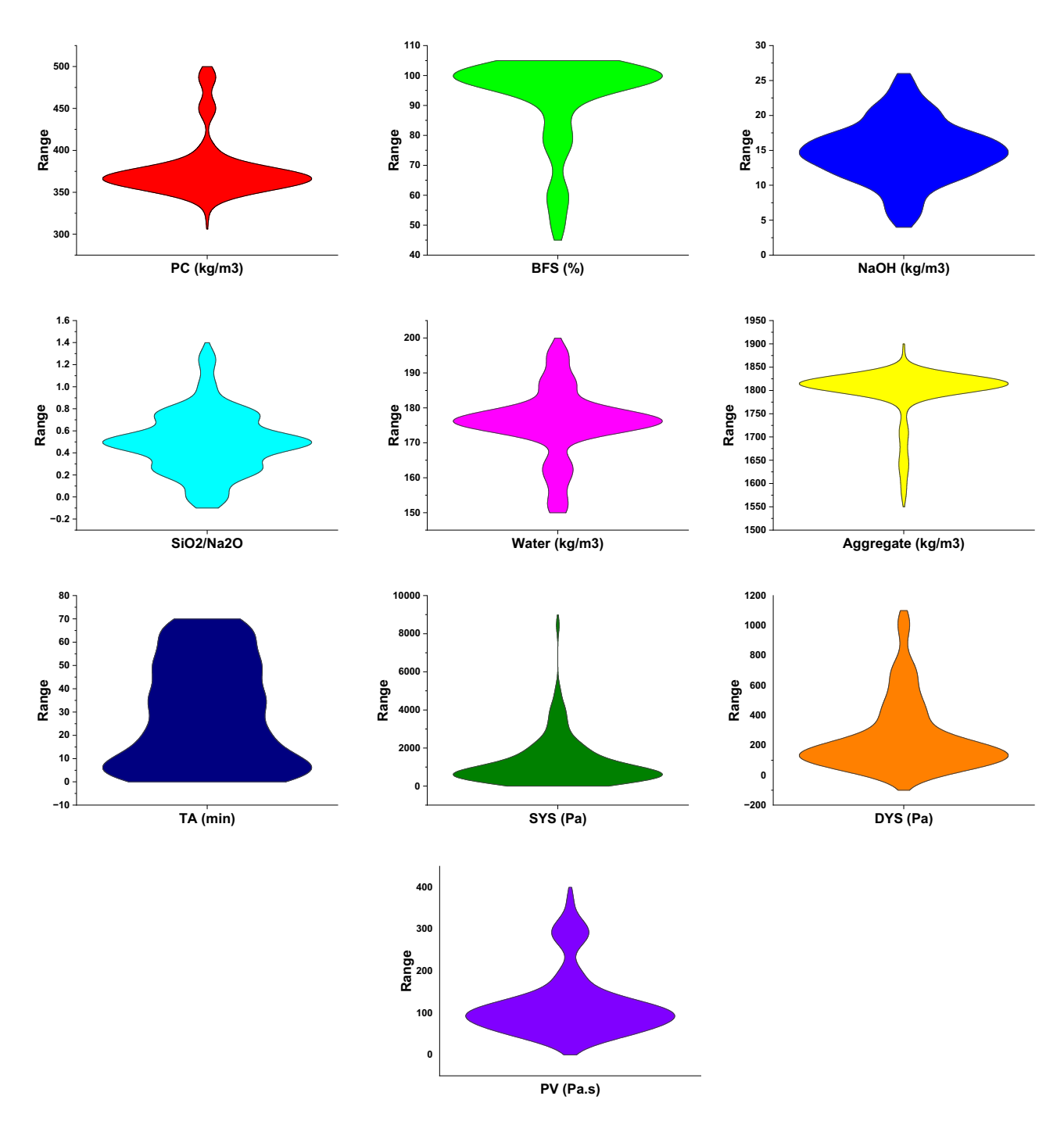


Figure 1: Violin diagrams depicting the input parameters' distributions.

the technique of reverse propagation. The weights of the model and the feedback losses are updated in an iterative manner through the application of gradient descent.

2.2.2 BE model

A comparable ensemble method best describes the process of incorporating new sets of training data into the forecast model. Asymmetric splitting is used to replace the actual set's values. Certain entries may be reproduced in each new set of substituting splitting utilized for the training data. Following bagging, each component's likelihood of being included in the updated data is equal. There has been no relation among the training set size and the accuracy of the predictions. A better approximation of the desired output may also significantly reduce the

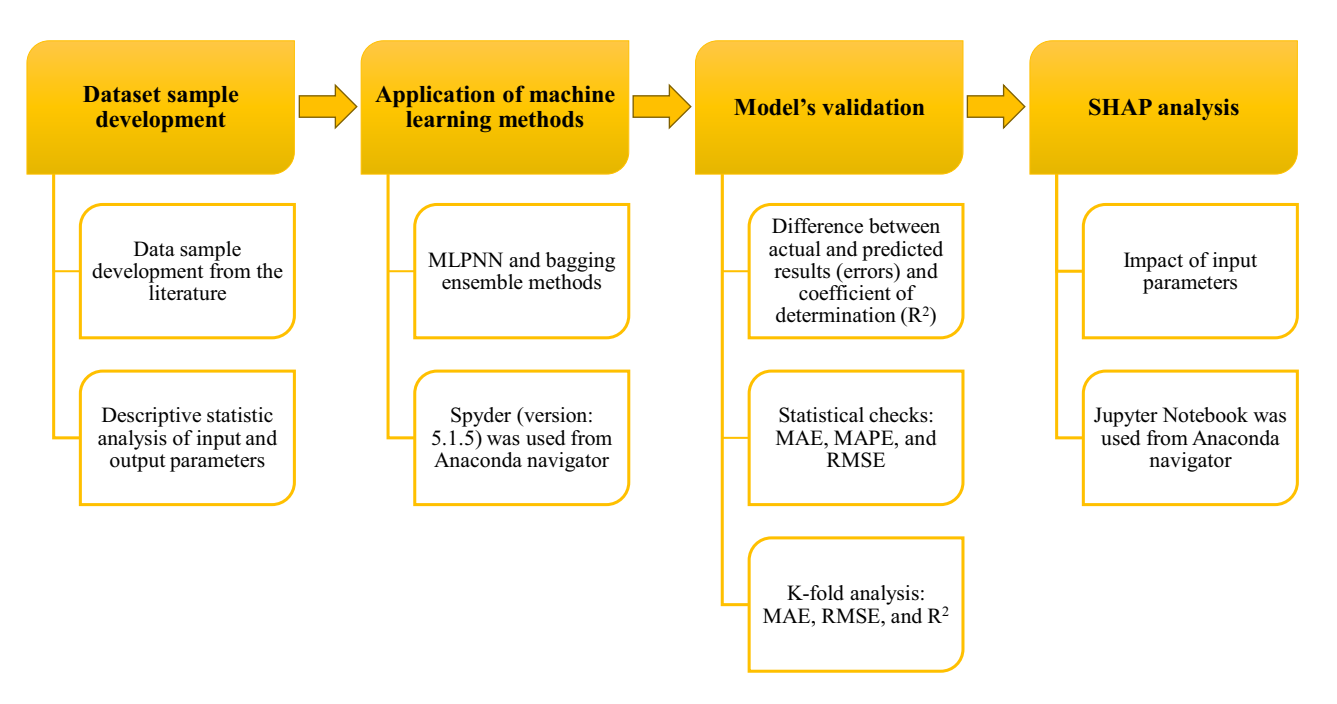


Figure 2: Data sample generation, modeling, and validation procedures flowchart.

divergence. This ensemble uses the typical forecast from all run simulations. Regression uses the median forecast from multiple simulations [39]. For the purpose of finetuning the MLPNN-based bagging strategy and determining its optimal output, 20 different models are utilized independently.

2.3 Validation of models

It was necessary to use k-fold techniques and number crunching in order to guarantee that the machine-learning simulations were accurate. After randomly partitioning the dataset into ten subgroups, the k-fold method is frequently utilized in order to evaluate the accuracy of a simulation [40]. Only one of the ten groups was employed for the actual testing of the ML models. When both the error and R^2 are modest, the ML algorithm performs at its best. The process also requires ten iterations before producing the expected outcome. This method substantially increases the model's accuracy for predictions. Statistical comparisons of the accuracy of various ML techniques were also made using error evaluation (mean absolute error [MAE], root mean squared error [RMSE], and mean absolute percentage error [MAPE]). Eqs. (1)-(3) were generated from previous work [41,42] and used to statistically verify the accuracy of the ML methods' estimates

MAE =
$$\frac{1}{n} \sum_{i=1}^{n} |P_i - T_i|,$$
 (1)

$$RMSE = \sqrt{\sum \frac{(P_i - T_i)^2}{n}},$$
 (2)

MAPE =
$$\frac{100\%}{n} \sum_{i=1}^{n} \frac{|P_i - T_i|}{T_i}$$
, (3)

where n is the data sample size, P_i is the predicted outcomes, and T_i is the actual value.

2.4 SHAP analysis

SHAP was proposed by Lundberg and Lee [43] to describe the additional feature attribute approach of machine learning. The process's input model is characterized by the linear sum of input variables. Let us assume that x is the model's input variable; for the original model f(x), the interpretation model g(x') of the streamlined input x' can be written as

$$f(x) = g(x') = \emptyset_0 + \sum_{i=1}^{M} \emptyset_i x_i'.$$
 (4)

In the absence of any features, \emptyset_0 is a constant equal to M, where M is the total number of input features. Each of \emptyset_0 , \emptyset_1 , \emptyset_2 , and \emptyset_3 will have a positive effect on the output variables since they raise the value of g(x), but \emptyset_4 has the reverse effect. There are a few distinct types of SHAP techniques, including kernel SHAP, Deep SHAP, and Tree SHAP. To better understand tree-based machine learning models like Bagging, tree SHAP [44] is employed here.

3 Results and analysis

3.1 MLPNN models

3.1.1 SYS MLPNN model

Figure 3 depicts the findings of employing the MLPNN method to forecast the SYS of AAC. In Figure 3(a), we see the connection between the tested SYS and the estimated SYS. The MLPNN method estimated SYS with only a reasonable level of precision and with moderate variance amongst tested and projected findings. There is an acceptable level of agreement between the real and estimated results when using the MLPNN approach to approximate the SYS of AAC ($R^2 = 0.88$). Figure 3(b) shows the actual, estimated, and absolute errors for the MLPNN. The mean absolute error value is 341.28 Pa, with a spread from 100.79 and 769.60 Pa. The proportionate breakdown of the errors also revealed that 8 readings were below 200 Pa, 29 were between 200 and 500 Pa, and 7 were beyond 500 Pa. The SYS of AAMs were accurately forecasted using the MLPNN method, as evidenced by the dispersion of errors. Additional statistical information is shown in Figure 4, which is a box plot and includes the following: minimum and maximum values, median, mean, and the standard deviation for both the experimental and projected test set outcomes. Values on the graph illustrate the disparity between the results that were predicted and those that were actually observed.

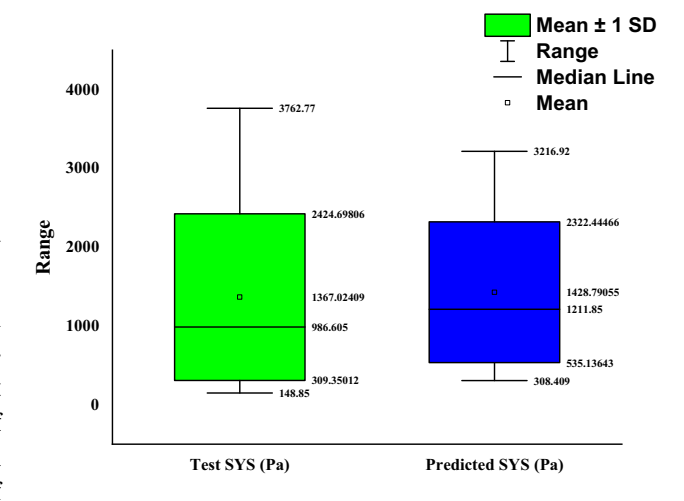
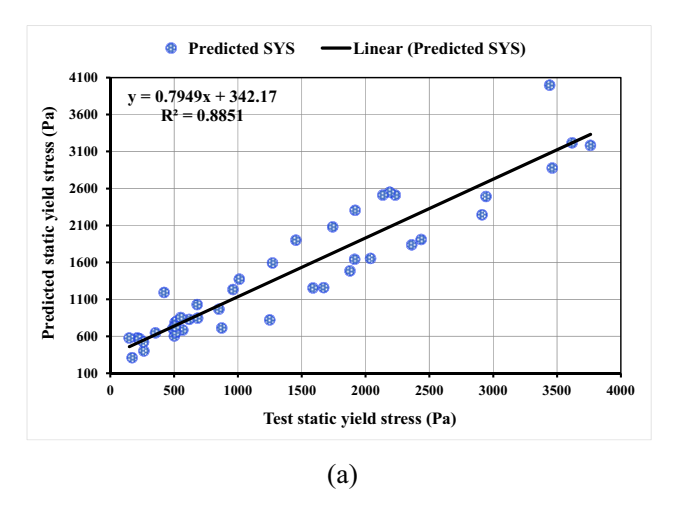


Figure 4: Comparison of the MLPNN-SYS model's predictions and experimental results in a box plot.

3.1.2 DYS MLPNN model

The results of estimating the DYS of AAC using the MLPNN technique are shown in Figure 5. In Figure 5(a), we see the connection between the tested DYS and the estimated SYS. The MLPNN method estimated DYS with only an acceptable level of precision and reduce deviation amongst actual and estimated results. It was established that the MLPNN strategy was effective in order to approximate the DYS of AAC; an R^2 value of 0.89 demonstrated that there was a better relation amongst the actual outcome and the MLPNN estimated findings for the DYS. A representation



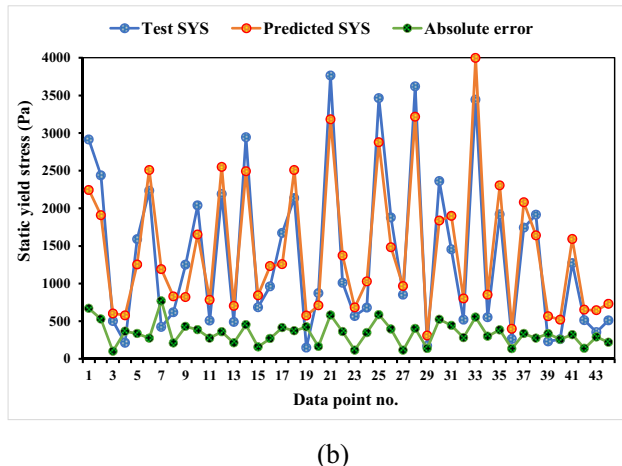
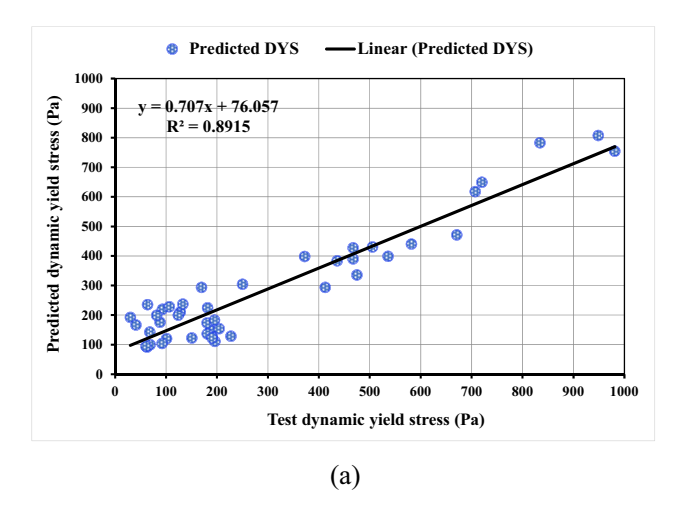


Figure 3: Model for MLPNN with SYS: (a) connection between SYS tests and predictions; and (b) distribution of SYS tests, predictions, and errors.



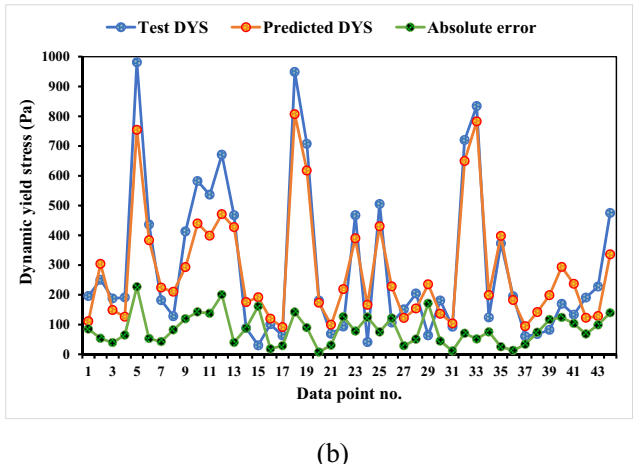


Figure 5: Model for MLPNN with DYS: (a) connection between DYS tests and predictions; and (b) distribution of DYS tests, predictions, and errors.

of the experimental, anticipated, and error dispersion for the MLPNN approach is shown in Figure 5(b). The mean error value is 83.63 Pa, with a spread between 7.62 and 226.84 Pa. Errors were also broken down proportionally, and it was determined that 13 values were less than 50 Pa, 16 were in between 50 and 100 Pa, and 15 were greater than 100 Pa. The MLPNN approach was able to accurately predict the DYS of AAMs, as seen by the spread of errors. Figure 6 is a box plot displaying extra statistical information. The findings from the test set, both experimental and anticipated, as well as the minimum, maximum, median, mean, and standard deviation values, are included in this report. Values on the graph illustrate the disparity between the results that were predicted and those that were actually observed.

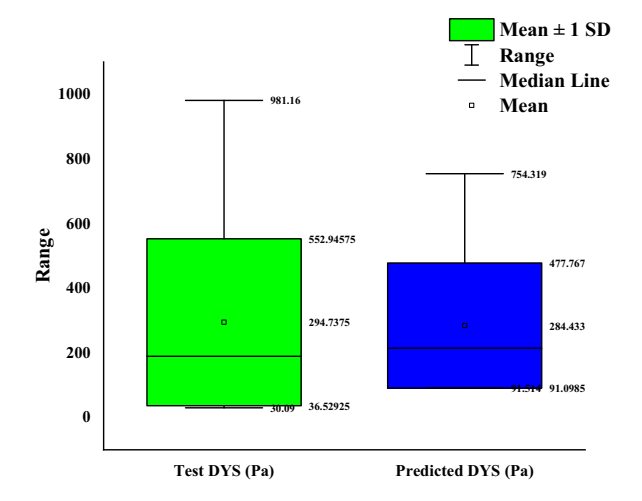


Figure 6: Comparison of the MLPNN-DYS model's predictions and experimental results in a box plot.

3.1.3 PV MLPNN model

Figure 7 shows the results of estimating the PV of AAC using the MLPNN approach. In Figure 7(a), we see the connection between the tested PV and the estimated SYS. The MLPNN method predicted PV with a reasonable level of precision, and with moderate difference between target and estimated results but slightly lesser accuracy in comparison to the MLPNN models for SYS and DYS. At an \mathbb{R}^2 of 0.86, a respectable degree of agreement was seen among the real and predicted results, suggesting that the MLPNN method was effective in estimating the AAC PV. Figure 7(b) displays the test, estimated, and absolute error spread for the MLPNN technique. The average absolute error value is 26.19 Pa·s, with a spread between 6.601 and 99.66 Pa·s. In addition, the errors were classified according to their proportions: 29 of the total values were found to be below 25 Pa·s. 8 were found to be between 25 and 50 Pa·s. and 7 were found to be greater than 100 Pa·s. Figure 8, which is a box plot, offers additional statistical details for the test set's experimental and predicted outcomes. These details include the minimum, maximum, median, mean, and standard deviation values. Values on the graph illustrate the disparity between the results that were predicted and those that were actually observed.

3.2 BE models

3.2.1 SYS BE model

A forecast of the AAC's SYS is shown in Figure 9, which displays the outcomes of adopting the BE method. The actual and predicted SYS are shown to have a correlation,

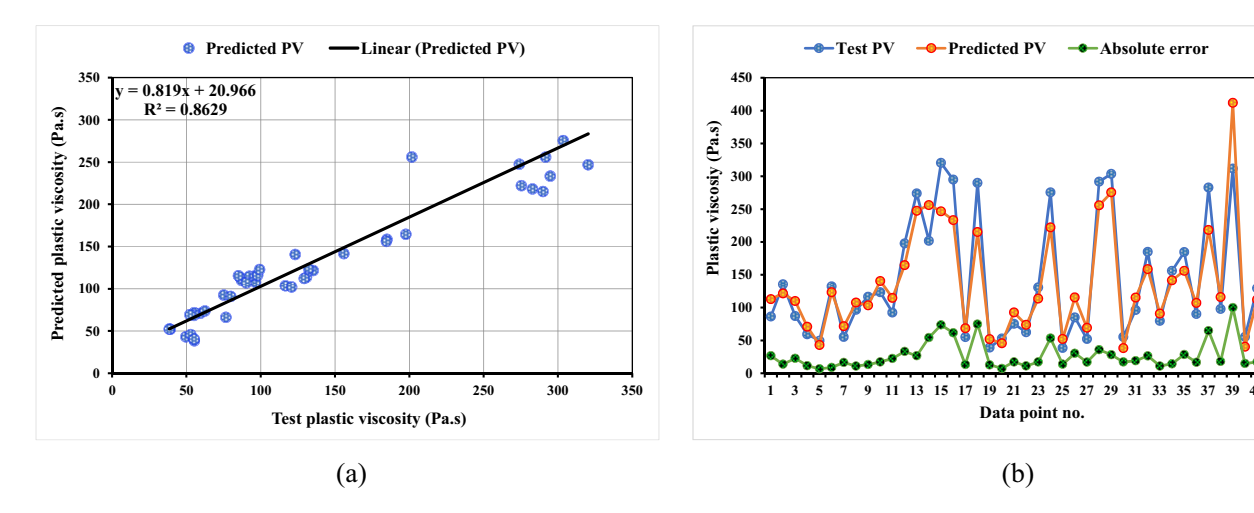


Figure 7: Model for MLPNN with PV: (a) connection between PV tests and predictions; and (b) distribution of PV tests, predictions, and errors.

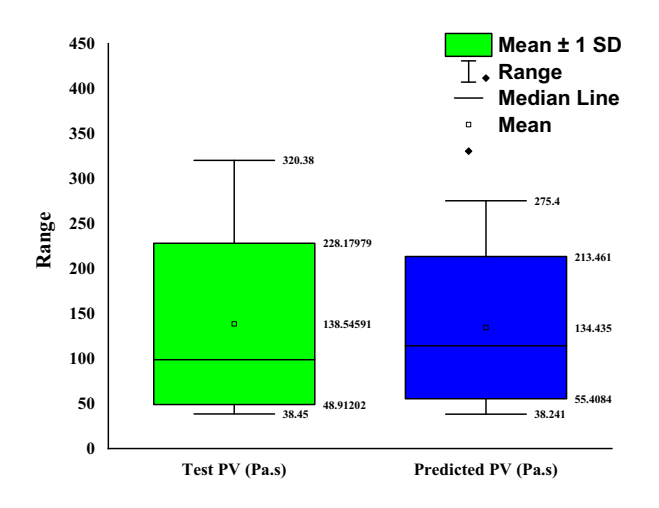


Figure 8: Comparison of the MLPNN-PV model's predictions and experimental results in a box plot.

as shown in Figure 9(a). The BE model yielded the least variations amongst real and model estimated findings, making it the more preferred ML method compared to the MLPNN method used. The BE method appears to be more precise because of its R^2 value of 0.95. The correlation of the BE method's error distribution for test, predicted, and error values is displayed in Figure 9(b). The findings exhibited that the least, average, and greatest absolute errors were 8.59, 228.58, and 598.54 Pa, respectively. The frequency of different-sized errors was analyzed, and it was discovered that 23 of the error values occurred at or below 200 Pa, 19 occurred between 200 and 500 Pa, and only 2 occurred at or above 500 Pa. According to the error dispersion, the BE model is likewise more precise than the MLPNN model. The BE model is found to be more accurate and effective than the MLPNN technique in determining the optimal output values because it utilizes 20 sub-

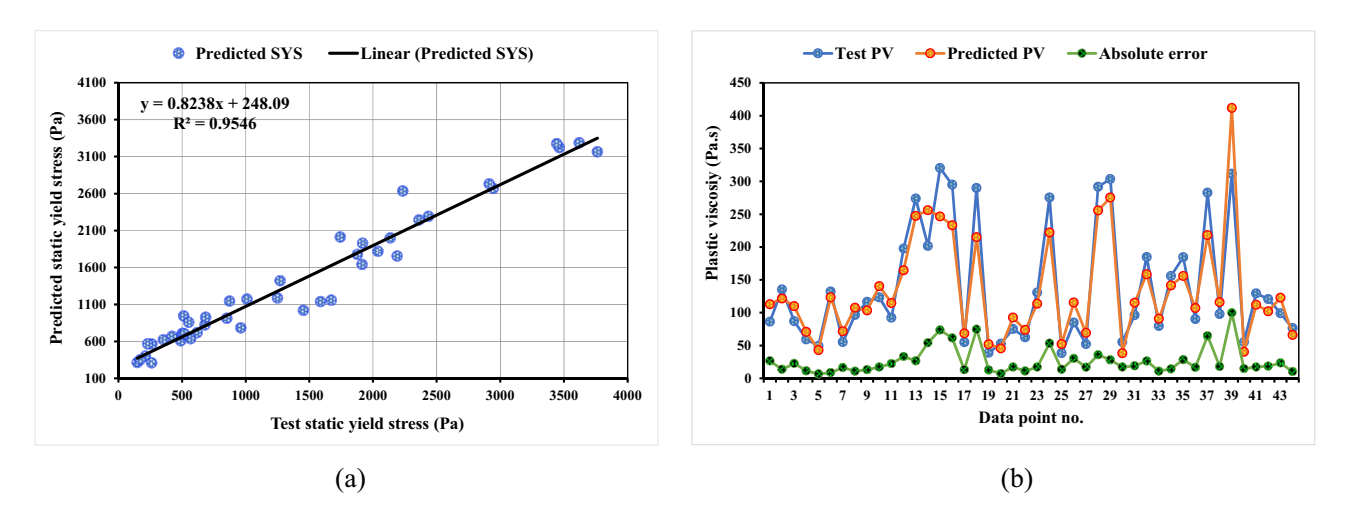


Figure 9: Model for BE with SYS: (a) connection between SYS tests and predictions; and (b) distribution of SYS tests, predictions, and errors.

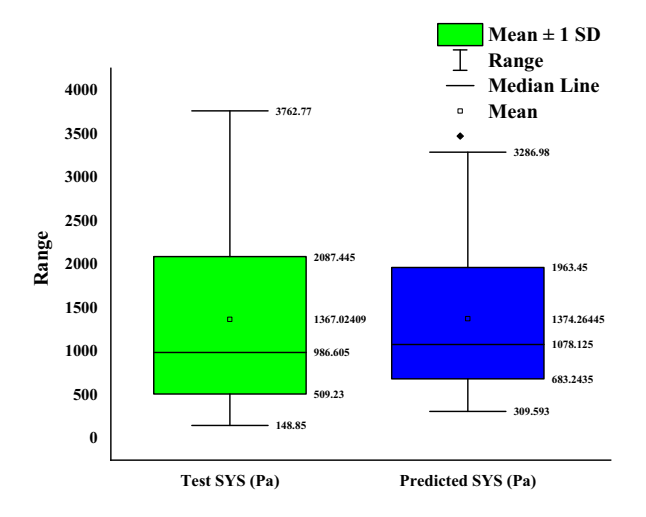


Figure 10: Comparison of the BE-SYS model's predictions and experimental results in a box plot.

models to fine-tune the bagging process. Additional statistical information is provided in Figure 10, which includes the experimental and predicted test sets' minimum, maximum, median, mean, and standard deviation values. The discrepancy between predictions and outcomes is shown by the numbers on the graph. Bagging model results appear more in line with one another (actual and anticipated) than MLPNN model results.

3.2.2 DYS BE model

The results of the BE approach to estimate the AAC's DYS are displayed in Figure 11. As shown in Figure 11(a), there is a correlation amongst experiment and projected DYS. The

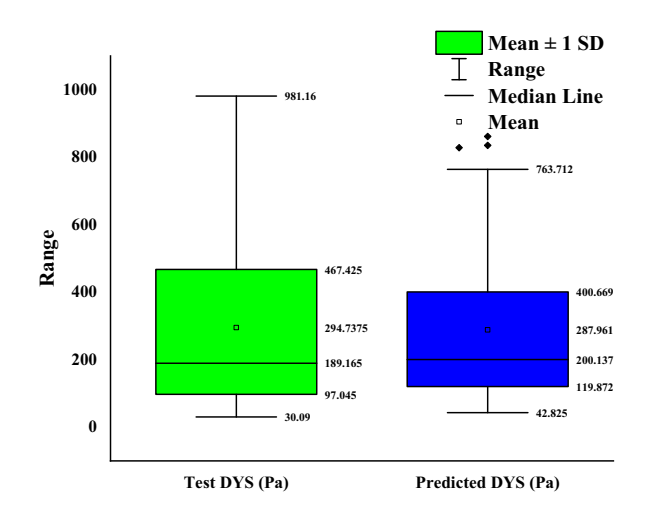
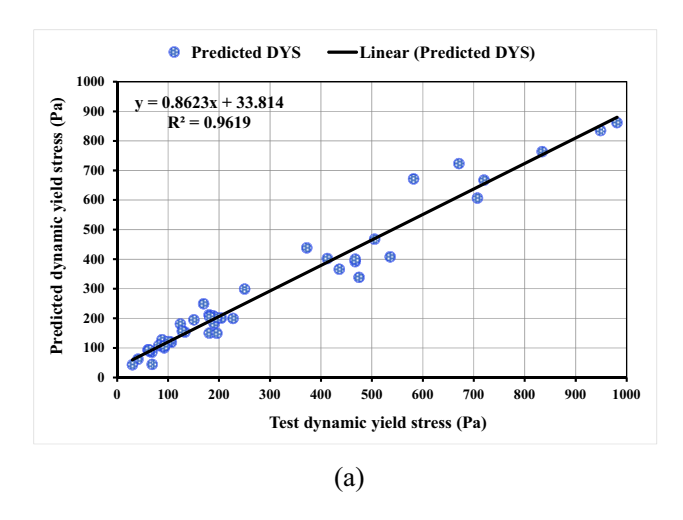


Figure 12: Comparison of the BE-DYS model's predictions and experimental results in a box plot.

BE model appears to be more precise because of its \mathbb{R}^2 value of 0.96. The illustration of the BE technique's error dispersal for test, predicted, and error values is depicted in Figure 11(b). The findings exhibited that the least, average, and maximum levels of absolute errors were 3.786, 44.56, and 136.86 Pa, respectively. The frequency of different-sized errors was analyzed, and it was discovered that 29 of the error values occurred at or below 50 Pa, 10 occurred between 50 and 100 Pa, and only 5 occurred at or above 100 Pa. The DYS-BE model was found to be more precise than the MLPNN model and equally accurate as the SYS-BE model in determining the optimal output. Additional statistical information is provided in Figure 12, which includes the experimental and predicted test sets' minimum, maximum, median, mean, and standard deviation values. The



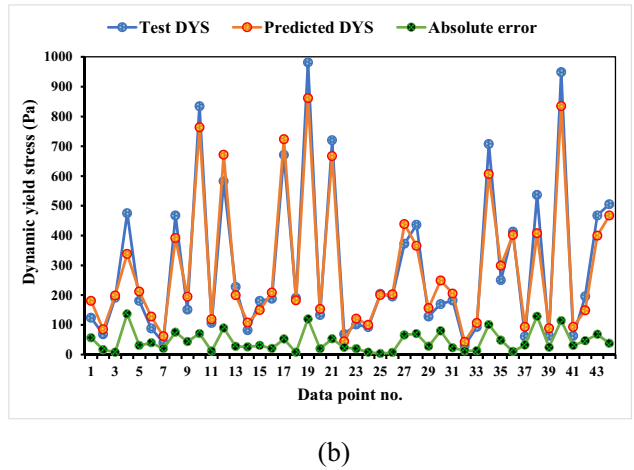


Figure 11: Model for BE with DYS: (a) connection between DYS tests and predictions; and (b) distribution of DYS tests, predictions, and errors.

values on the graph illustrate the gap between forecasts and actual results. Bagging model results appear more in line with one another (actual and anticipated) than MLPNN model results.

3.2.3 PV BE model

The results of employing the BE approach to predict the AAC's PV are given in Figure 13. As shown in Figure 13(a), there is a correlation amongst target and estimated PV. The BE model appears to be more accurate due to its R^2 value of 0.93, slightly less than the R^2 of the BE model for SYS and DYS. The illustration of the BE model's error dispersal for actual, estimated, and error values is depicted in Figure 13(b). The findings exhibited that the least, average, and maximum levels of error were 0.53, 23.28, and 70.66 Pa·s. The frequency of different-sized errors was analyzed, and it was discovered that 30 of the error values occurred at or below 23 Pa·s, 9 occurred between 25 and 50 Pa·s, and only 5 occurred at or above 50 Pa·s. The DYS-PV model was found to be more precise than the MLPNN model and marginally less accurate than the SYS and DYS BE models in forecasting the desired outcomes. Additional statistical information is provided in Figure 14, which includes the experimental and predicted test sets' minimum, maximum, median, mean, and standard deviation values. The values on the graph illustrate the gap between forecasts and actual results. Bagging model results appear more in line with one another (actual and anticipated) than MLPNN model results.

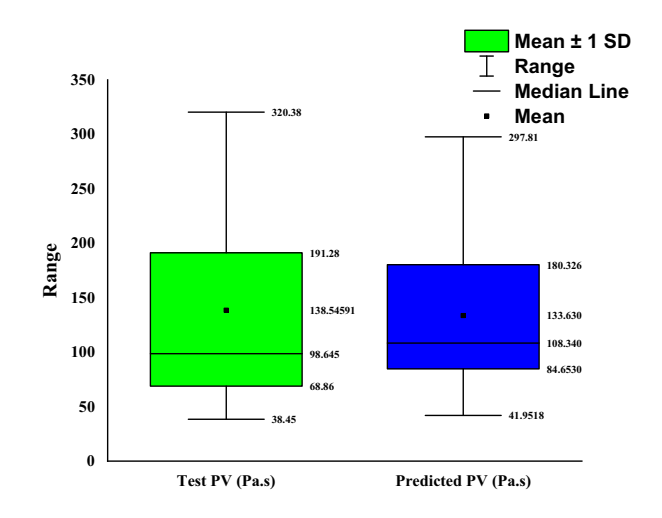
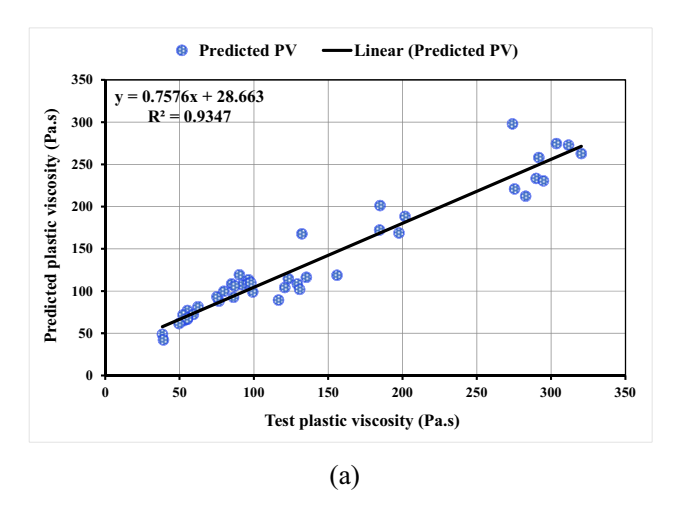


Figure 14: Comparison of the BE-PV model's predictions and experimental results in a box plot.

3.3 Model's validation

The results of the error computations (MAE, RMSE, and MAPE) that were performed using Eqs. (1)–(3) that were previously described are presented in Table 2. It was found that the MLPNN and BE models had MAE values of 341.28 and 228.59 Pa, respectively, while predicting SYS. However, for forecasting DYS, MLPNN had an MAE value of 83.63 Pa, and BE had an MAE value of 20.80 Pa. Similarly, in the case of PV prediction, MLPNN and BE model's MAE were found to be 26.20 and 23.29 Pa·s. MAPE was calculated to be 46.30% for MLPNN and 32.70% for BE model while



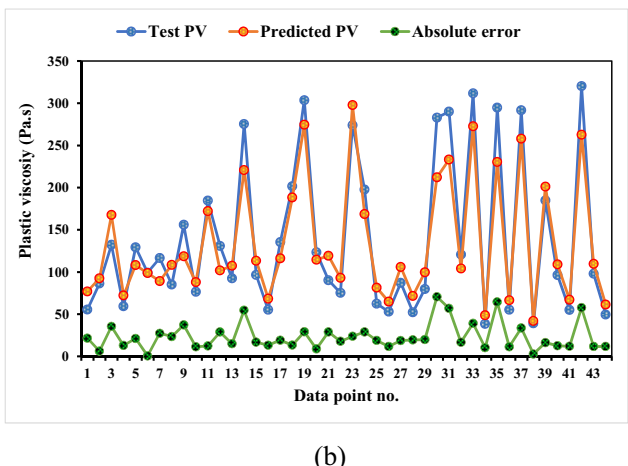


Figure 13: Model for BE with PV: (a) connection between PV tests and predictions; and (b) distribution of PV tests, predictions, and errors.

Table 2: Statistical analyses for assessing errors

ML Technique	SYS				DYS		PV			
	MAE (Pa)	MAPE (%)	RMSE (Pa)	MAE (Pa)	MAPE (%)	RMSE (Pa)	MAE (Pa·s)	MAPE (%)	RMSE (Pa·s)	
MLPNN	341.28	46.30	373.53	83.63	62.00	98.29	26.20	19.90	33.33	
Bagging	228.59	32.70	263.18	44.56	20.80	56.56	23.29	18.60	28.29	

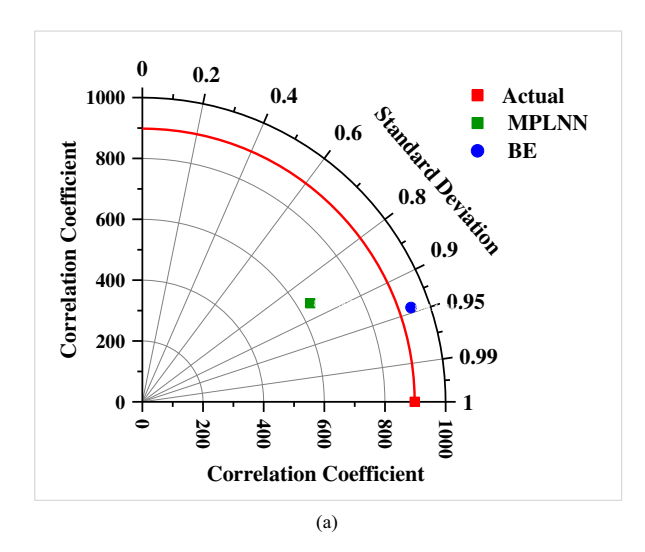
predicting SYS, whereas the MAPE value was 62.00 and 20.80% for DYS forecasting MLPNN and BE models, respectively. In the case of PV, MAPE was found to be 19.90 and 18.60% for MLPNN and BE models, correspondingly. The root-mean-square error (RMSE) values for SYS-based MLPNN and BE models were also calculated to be 373.53 and 263.18 Pa, respectively. RMSE values were 98.29 and 56.56 Pa for MLPNN and BE models, respectively, for DYS prediction. Similarly, for PV forecasting models, MLPNN and BE had RMSE values of 33.33 and 28.29 Pa·s, respectively. All these statistical results show the higher accuracy of prediction of BE models over MLPNN models in all three cases, as the error rate significantly decreases.

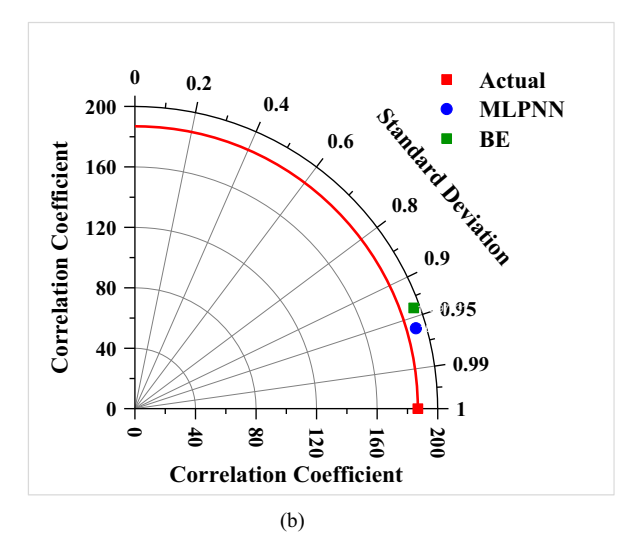
Table 3 displays the results of computing \mathbb{R}^2 , RMSE, and MAE, which were used to validate the k-fold approach. The MLPNN and BE methods produced an SYS estimate with an MAE of 372.90 and 273.60 Pa, respectively. DYS-based MLPNN and BE models had average MAE values of 83.18 and 55.69 Pa, respectively. MAE mean values of 36.15 and

32.69 Pa·s were found in the case of PV-prediction MLPNN and BE models. The MLPNN had an RMSE averaging 418.63 Pa, 98.40 Pa, and 45.13 Pa·s for SYS, DYS, and PV prediction, respectively. However, in the case of BE modeling, mean RMSE values of 365.23 Pa, 72.70 Pa, and 41.70 Pa·s were found for SYS, DYS, and PV outcomes, respectively. MLPNN and BE had maximum R^2 values of 0.89 and 0.95 for SYS, whereas 0.89 and 0.96 maximum R^2 for DYS, respectively. Maximum R^2 values of 0.87 and 0.93 were found for MLPNN and BE models for PV estimation, respectively. The finest BE model for predicting the SYS, DYS, and PV of AAC had a higher R^2 and lower errors. The improved precision of BE models was also confirmed by analyzing errors and R² values noted from the k-fold analysis. However, the exactness of the MLPNN models was also in satisfactory limits. As a result, MLPNN and BE models may provide better estimates of AAC's SYS, DYS, and PV. All the existing forecasting models are compared in Figure 15, which is a Taylor diagram. With regard to all three cases

Table 3: Outcomes of MAE, RMSE, R^2 from k-fold analysis

Property	ML model	Parameter	k-fold no.									
			1	2	3	4	5	6	7	8	9	10
SYS	MLPNN	MAE	151.99	807.51	536.43	367.19	256.43	402.98	132.94	516.52	232.68	334.36
		RMSE	412.17	960.24	506.62	305.06	271.51	513.02	242.62	431.77	302.23	241.04
		R^2	0.43	0.57	0.42	0.46	0.63	0.89	0.58	0.61	0.53	0.25
	BE	MAE	203.79	116.30	336.02	278.97	235.47	605.49	304.07	252.52	125.17	278.21
		RMSE	298.44	224.01	848.77	324.29	283.67	427.10	443.32	178.48	386.21	237.96
		R^2	0.61	0.59	0.76	0.70	0.48	0.35	0.95	0.60	0.59	0.46
DYS	MLPNN	MAE	245.85	44.51	57.13	69.29	70.71	90.50	75.17	64.86	95.25	18.49
		RMSE	308.89	83.40	86.75	38.47	80.41	84.71	102.89	70.89	96.76	30.81
		R^2	0.59	0.59	0.23	0.44	0.62	0.31	0.89	0.59	0.44	0.53
	BE	MAE	12.72	174.45	51.25	35.13	48.27	61.72	46.91	72.28	20.32	33.88
		RMSE	206.66	89.80	22.13	74.54	57.49	94.89	41.74	51.57	31.85	56.33
		R^2	0.96	0.68	0.59	0.31	0.38	0.55	0.30	0.74	0.52	0.45
PV	MLPNN	MAE	27.35	25.26	22.76	90.98	45.44	32.54	37.86	17.30	33.65	28.34
		RMSE	98.64	41.35	38.91	54.00	42.67	40.42	42.36	22.96	33.19	36.78
		R^2	0.33	0.29	0.25	0.20	0.23	0.87	0.46	0.62	0.56	0.38
	BE	MAE	38.21	23.04	27.72	68.13	44.83	26.59	27.98	14.92	30.27	25.19
		RMSE	95.08	48.13	29.35	44.52	35.95	47.98	18.98	36.41	28.75	32.78
		R^2	0.49	0.68	0.57	0.29	0.48	0.29	0.65	0.62	0.44	0.93





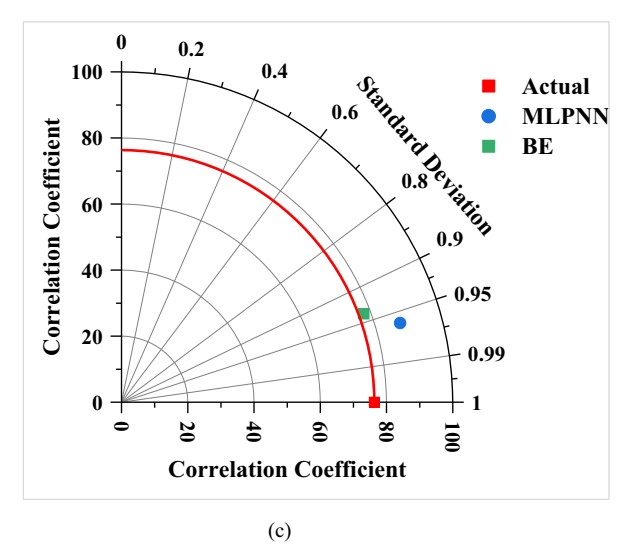


Figure 15: Taylor diagram: (a) SYS; (b) DYS; and (c) PV.

(SYS, DYS, and PV), the bagging models stand out as the most nearby, while the MLPNN models are the most distant.

3.4 SHAP analysis results

This research scrutinized how input parameters affected the rheological properties of AAC. Local SHAP and feature impacts are clarified by the SHAP tree explainer for the entire dataset. Figures 16–18 show the violin SHAP graph's results for all raw materials on AAC rheology. Each variable value in this graph is colored, and the x-axis SHAP value shows each raw material's influence. As depicted in Figure 16, PC, TA, BFS, and aggregate all these input parameters have a positive correlation with the SYS of AAC. SYS, which is the effort required to initiate flow in concrete, increases as the content of the above-mentioned parameters increases. However, water, SiO₂/Na₂O, and NaOH parameters have a more negative correlation with the SYS of AAC, which means that increasing the content of these variables might result in a decrease in the SYS of the AAC. Figure 17 illustrates the SHAP plot of input parameters for DYS. TA, aggregate, and BFS parameters have a positive correlation with DYS, which is the minimum effort required to maintain the flow of concrete. However, the relation of parameters PC and SiO₂/Na₂O with DYS of AAC was more negative, which means that the DYS decreases with the increase in the content of these variables. Furthermore, the NaOH and water correlation with DYS of AAC was balanced (both equally positive and negative). SHAP plot for PV correlation with the input parameters is shown in Figure 18, illustrating that the BFS. water, and SiO₂/Na₂O have a more direct relationship with the PV of AAC. However, the relationship of PC with the PV of AAC was found to be more adverse. Furthermore, NaOH, aggregate, and TA relationship with PV were found to be equally positive and negative, suggesting that their content increase might have a positive/negative impact on the PC of AAC.

The SHAP approach exhibits a remarkable insight into the interactions among input features, effectively demonstrating the collective impact of several factors on predictions. An integrated approach is required for realizing complex correlations within ML models, as they might not be effectively identifiable using correlation analysis alone [35]. The color representation is used to Display the

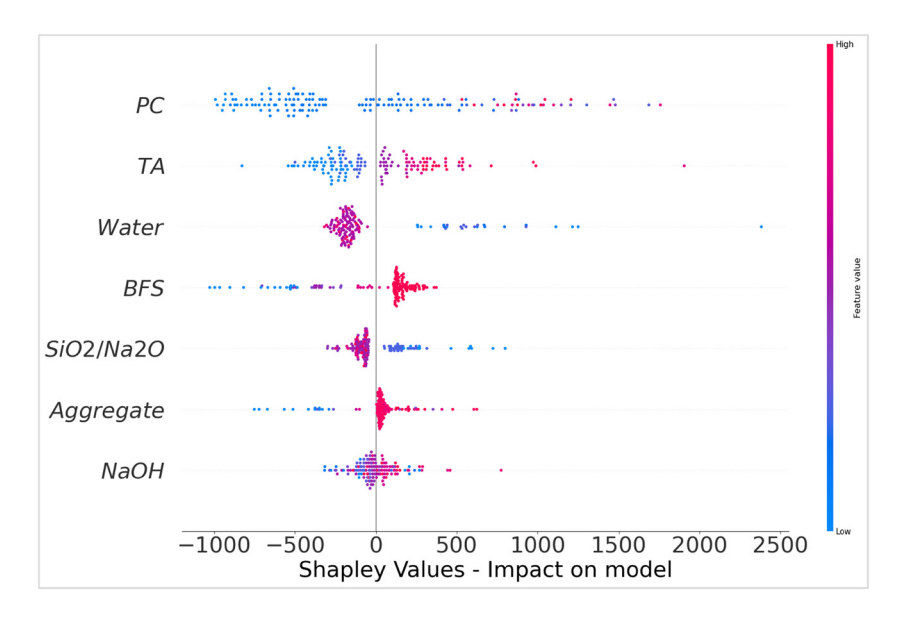


Figure 16: SHAP plot for SYS.

level of correlation amongst two variables for each individual parameter. In Figure 19, each dot is displayed with red to imply a high score of the most dependent variable, and a blue shade is displayed to represent a low value of the most dependent variable. The graph primarily depicts the correlation between the values of a specific variable and the related SHAP values. There is a direct correlation between the output of the model and the PC, which reaches its highest point at 375 kg·m⁻³, as shown in Figure 19(a). Figure 19(b) and (c) shows that the output values increase as the amount of BFS and NaOH in the mixture increases. On the other hand, Figure 19(d) and (e) illustrates an indirect link between SiO₂/Na₂O and water, which indicates a significant decrease in output with increasing content. Following that, Figure 19(f) and (g) illustrates the positive correlations that exist between the aggregate content, the TA, and subsequent outputs. The fact that these conclusions are dependent on particular raw materials and data samples is an extremely important consideration to take into account. Variations in the parameters and data that are entered could potentially result in different outcomes.

4 Discussions

Traditional binding ingredient, OPC has a great global impact based on both raw material Consumption [45] and anthropogenic releases [46]. As a result, the OPC industry needs to establish environmentally preferable alternatives to OPC in order to cut down on the amount of

carbon dioxide emissions it produces. Because of their low impact on the environment and low energy consumption, AAMs, also known as AAMs, have garnered a lot of attention over the past 10 years as one of the most advantageous building materials [47]. Through the application of ML and SHAP methodologies, the purpose of this study was to further human comprehension of the application of AAMs. This study used MLPNN, and BE ML approaches to estimate the SYS, DYS, and PV of AAC. To determine which method is the most precise predictor, the accuracy of each method was compared. The BE approach yielded more accurate findings than the MLPNN technique, with an \mathbb{R}^2 of 0.95 for SYS, 0.96 for DYS, and 0.93 for PV. The MLPNN techniques had an R^2 of 0.88 for SYS, 0.89 for DYS, and 0.86 for PV. The discrepancy between actual and predicted results (errors) supported the BE approach's higher accuracy even further. In contrast to the MLPNN models, the BE models' experimental and predicted results agreed quite well, as shown by the error analysis. Similar findings from earlier research have demonstrated that the BE methodology is superior to the individual ML methods in terms of accuracy when it comes to calculating the strength of construction materials [41,48].

In addition, ML methods were tested for accuracy using both arithmetical and k-fold approaches. A smaller amount of deviation (RMSE, MAPE, and MAE) and a higher R^2 indicate that the model is more accurate. Algorithm performance depends on inputs and data samples, making it difficult to identify the optimal machine-learning method for attribute prediction across domains [41]. Ensemble ML

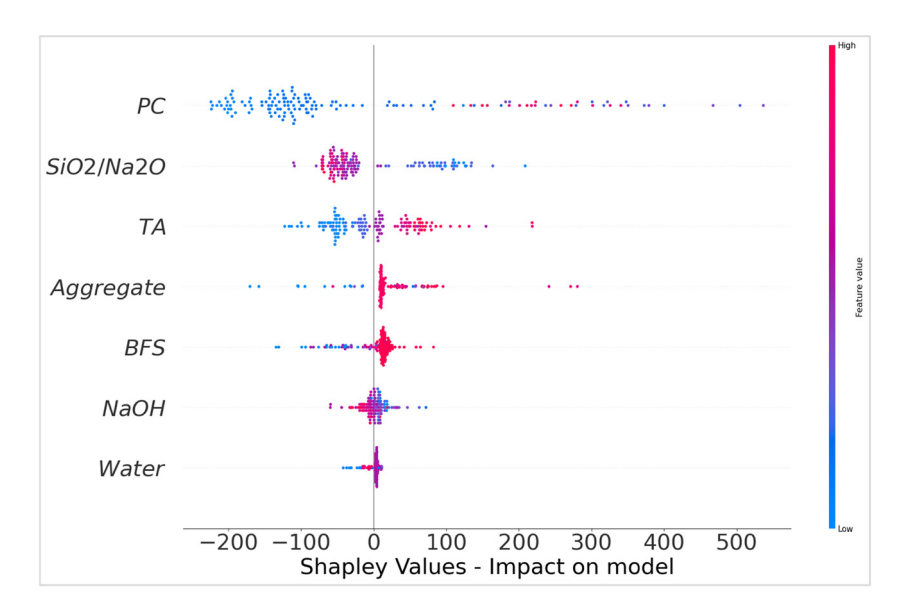


Figure 17: SHAP plot for DYS.

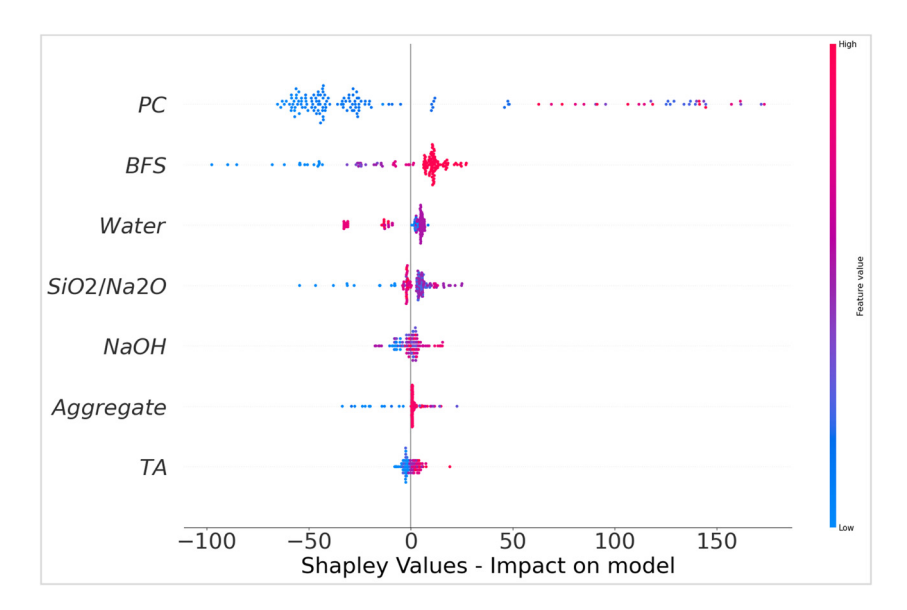


Figure 18: SHAP plot for PV.

approaches often use the weaker learner to train submodels on the dataset and tune them to improve accuracy, resulting in outputs that surpass individual ML models. All things considered, these outcomes show that BE models are more accurate than MLPNN models. Additionally, the SHAP analysis was performed to look at how raw materials interact and affect the rheological aspects of AAC. The SYS of AAC is positively correlated with the PC, TA, BFS, and aggregate of the input parameters used to create the material. The amount of work needed to commence flow in concrete, denoted by the parameter SYS, grows as the content of the aforementioned variables does. However, DYS, TA,

aggregate, and BFS parameters have a positive correlation with DYS, which is the minimum effort required to maintain the flow of concrete. There is a stronger correlation between the PV of AAC and the BFS, water, and SiO₂/Na₂O. However, a greater negative correlation was observed between PC and PV for AAC. Therefore, it can be concluded that using AAMs as an alternative to OPC-based materials will result in better construction materials having comparatively similar strength-wise performance. Moreover, more importantly, it will help reduce the environmental concerns associated with OPC production and also control the depleting raw materials used in OPC creation.

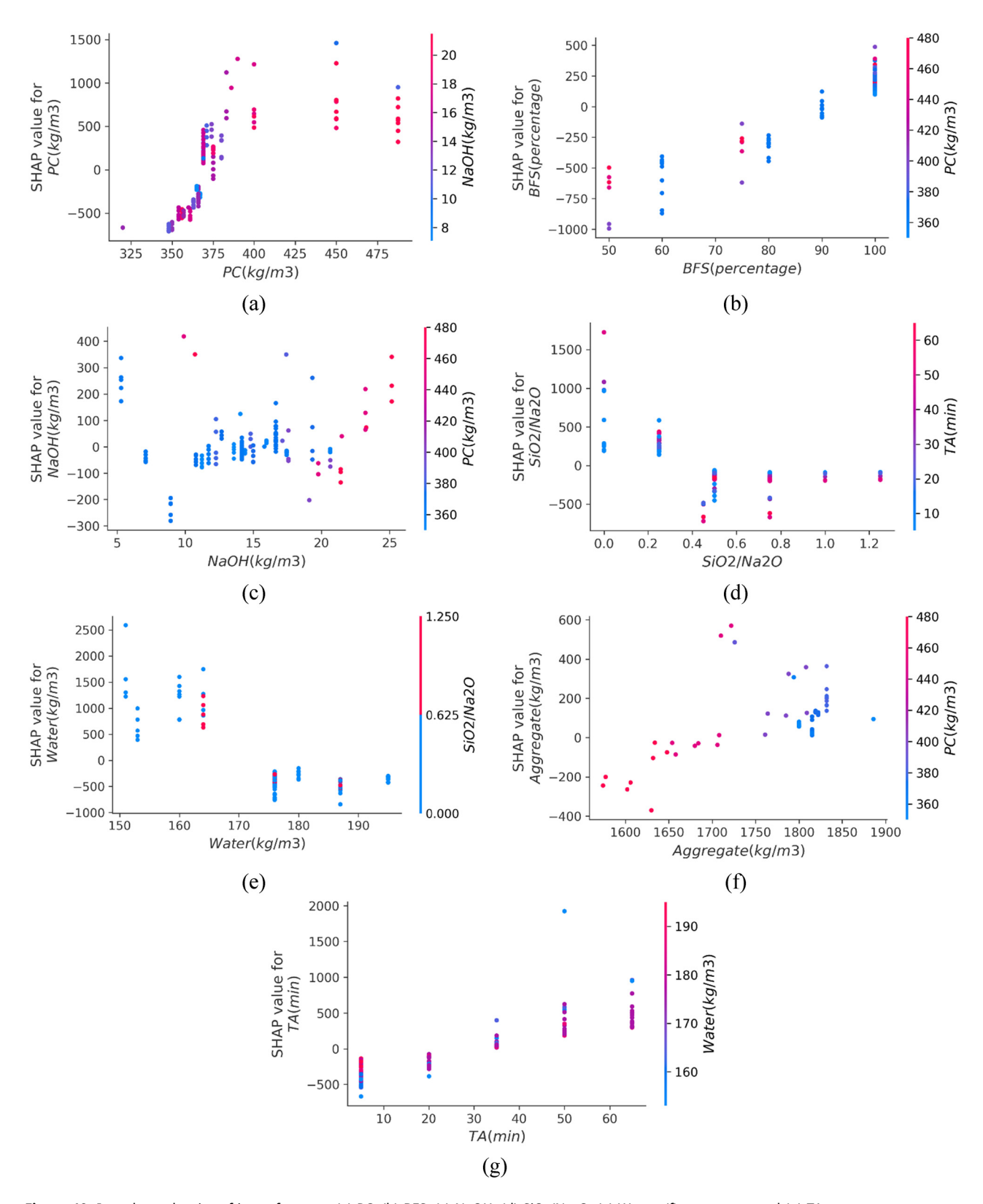


Figure 19: Interdependencies of input features: (a) PC; (b) BFS; (c) NaOH; (d) SiO₂/Na₂O; (e) Water; (f) aggregate; and (g) TA.

5 Conclusions

AAC rheological properties were the focus of this research, which developed prediction models using MLPNN and BE. The generated models were trained and validated using 145 rheological data (yield stress [static/dynamic] and PV). The primary outcomes of the research are as follows:

- The MLPNN models correctly predicted the rheological parameters of AAC, including SYS, DYS, and PV, with R^2 values of 0.88, 0.89, and 0.87. BE models predicted SYS, DYS, and PV better with R^2 values of 0.95, 0.96, and 0.93.
- The average error between experimental and projected SYS, DYS, and PV in MLPNN techniques was 341.28 Pa, 83.63 Pa, and 26.19 Pa·s. However, BE models lowered average error values to 228.58 Pa, 44.56 Pa, and 23.28 Pa·s for SYS, DYS, and PV prediction. These error rates confirmed that MLPNN models were accurate and BE approaches predicted AAC rheology better.
- Statistical and k-fold evaluations confirmed the effectiveness of the created models. Better R² and fewer mistakes showed ML model accuracy. MLPNN models predicted SYS, DYS, and PV with MAPEs of 46.20, 62.00, and 19.90%. In BE models for SYS, DYS, and PV, MAPE values dropped to 32.0, 20.80, and 18.890%. BE models had lower MAE and RMSE values than MLPNN models, demonstrating their improved AAC rheology prediction.
- There was a strong positive correlation between the SHAP analysis and the SYS of AAC, and the two most important input characteristics were TA and PC. However, in the DYS prediction, as per the SHAP analysis, TA and aggregate were the most influential parameters. PV of AAC was more positively impacted by the BFS and water based on the SHAP analysis.

Future research may focus on adding experimental data to increase model accuracy. The study used MLPNN and BE models. However, future research could examine single and ensemble techniques like SVM, DT, and boosting, as well as hybrid ML techniques like GA-PSO and RF-ANN. The models' functionality and predictive abilities might benefit greatly from including these hybrid approaches. Also, research into the AAC's durability, dynamic characteristics (fatigue), and microstructure is lacking, and a deeper exploration of these longevity determinants *via* ML approaches is required.

Acknowledgments: The authors would like to express their deepest gratitude to the Scientific Research Deanship and to the College of Engineering at the University of Ha'il-Saudi Arabia, for providing necessary support for conducting this research, through project number RG-23 062.

Funding information: This research has been funded by Scientific Research Deanship at University of Ha'il – Saudi Arabia through project number RG-23 062.

Author contributions: M.N.A.: conceptualization, project administration, funding acquisition, investigation, writing, reviewing, and editing. A.A-N.: resources, formal analysis, funding acquisition, writing, reviewing, and editing. R-U-D.N.: visualization, resources, writing, reviewing, and editing. O.A.: conceptualization, methodology, investigation, writing, reviewing, and editing. S.A.K.: data acquisition, software, validation, methodology, writing-original draft. A.F.D.: software, investigation, writing, reviewing, and editing. All authors have accepted responsibility for the entire content of this manuscript and approved its submission.

Conflict of interest: The authors state no conflict of interest.

Data availability statement: The datasets generated and/ or analyzed during the current study are available from the corresponding author upon reasonable request.

References

- [1] Singh, N. B., M. Kalra, and S. K. Saxena. Nanoscience of cement and concrete. *Materials Today: Proceedings*, Vol. 4, 2017, pp. 5478–5487.
- [2] Scrivener, K. L. Options for the future of cement. *Indian Concrete Journal*, Vol. 88, 2014, pp. 11–21.
- [3] Herrmann, A., A. Koenig, and F. Dehn. Structural concrete based on alkali-activated binders: Terminology, reaction mechanisms, mix designs and performance. *Structural Concrete*, Vol. 19, 2018, pp. 918–929.
- [4] Duxson, P. and J. L. Provis. Designing precursors for geopolymer cements. *Journal of the American Ceramic Society*, Vol. 91, 2008, pp. 3864–3869.
- [5] Gislason, S. R. and E. H. Oelkers. Mechanism, rates, and consequences of basaltic glass dissolution: II. An experimental study of the dissolution rates of basaltic glass as a function of pH and temperature. *Geochimica et Cosmochimica Acta*, Vol. 67, 2003, pp. 3817–3832.
- [6] Provis, J. L. and J. S. J. van Deventer. RILEM state-of-the-art reports state-of-the-art report, RILEM TC 224-AAM, 2014.
- [7] Provis, J. L., A. Palomo, and C. Shi. Advances in understanding alkali-activated materials. *Cement and Concrete Research*, Vol. 78, 2015, pp. 110–125.
- [8] Provis, J. L. Activating solution chemistry for geopolymers. In *Geopolymers*, Elsevier, Cambridge, UK, 2009, pp. 50–71.
- [9] Provis, J. L. Geopolymers and other alkali activated materials: why, how, and what? *Materials and Structures*, Vol. 47, 2014, pp. 11–25.
- [10] van Deventer, J. S. J., R. San Nicolas, I. Ismail, S. A. Bernal, D. G. Brice, and J. L. Provis. Microstructure and durability of alkali-activated materials as key parameters for standardization. *Journal of Sustainable Cement-Based Materials*, Vol. 4, 2015, pp. 116–128.

- Michalski, R. S., J. G. Carbonell, and T. M. Mitchell. Machine learning: An artificial intelligence approach, Springer Science & Business Media, Heidelberg, Germany, 2013.
- [12] Luger, G. F. Artificial intelligence: structures and strategies for complex problem solving, Pearson Education, Boston, USA, 2005.
- [13] Chadaga, K., S. Prabhu, N. Sampathila, R. Chadaga, and M. Bairy. An explainable framework to predict child sexual abuse awareness in people using supervised machine learning models. *Journal of* Technology in Behavioral Science, 2023, pp. 1–17.
- [14] Chadaga, K., S. Prabhu, V. Bhat, N. Sampathila, S. Umakanth, and R. Chadaga. Artificial intelligence for diagnosis of mild-moderate COVID-19 using haematological markers. Annals of Medicine, Vol. 55, 2023, id. 2233541.
- [15] Khanna, V. V., K. Chadaga, N. Sampathila, R. Chadaga, S. Prabhu, K. S. Swathi, et al. A decision support system for osteoporosis risk prediction using machine learning and explainable artificial intelligence. Heliyon, Vol. 9, 2023.
- [16] Amin, M. N., W. Ahmad, K. Khan, M. N. Al-Hashem, A. F. Deifalla, and A. Ahmad. Testing and modeling methods to experiment the flexural performance of cement mortar modified with eggshell powder. Case Studies in Construction Materials, Vol. 18, 2023, id. e01759.
- [17] Wang, N., M. Samavatian, V. Samavatian, and H. Sun. Bayesian machine learning-aided approach bridges between dynamic elasticity and compressive strength in the cement-based mortars. Materials Today Communications, Vol. 35, 2023, id. 106283.
- [18] Li, Q. and Z. Song. Prediction of compressive strength of rice husk ash concrete based on stacking ensemble learning model. Journal of Cleaner Production, Vol. 382, 2023, id. 135279.
- [19] Wang, N., Z. Xia, M. N. Amin, W. Ahmad, K. Khan, F. Althoey, et al. Sustainable strategy of eggshell waste usage in cementitious composites: An integral testing and computational study for compressive behavior in aggressive environment. Construction and Building Materials, Vol. 386, 2023, id. 131536.
- [20] Amin, M. N., B. Iftikhar, K. Khan, M. F. Javed, A. M. AbuArab, and M. F. Rehman. Prediction model for rice husk ash concrete using AI approach: Boosting and bagging algorithms. In Structures, Elseiver, 2023. pp. 745-757.
- [21] Sun, Y., H. Cheng, S. Zhang, M. K. Mohan, G. Ye, and G. De Schutter. Prediction & optimization of alkali-activated concrete based on the random forest machine learning algorithm. Construction and Building Materials, Vol. 385, 2023, id. 131519.
- [22] Amin, M. N., H. A. Alkadhim, W. Ahmad, K. Khan, H. Alabduljabbar, and A. Mohamed. Experimental and machine learning approaches to investigate the effect of waste glass powder on the flexural strength of cement mortar. PloS one, Vol. 18, 2023, id. e0280761.
- [23] Zheng, X., Y. Xie, X. Yang, M. N. Amin, S. Nazar, S. A. Khan, et al. A data-driven approach to predict the compressive strength of alkaliactivated materials and correlation of influencing parameters using SHapley Additive exPlanations (SHAP) analysis. Journal of Materials Research and Technology, Vol. 25, 2023, pp. 4074-4093.
- Ke, X. and Y. Duan. Coupling machine learning with thermodynamic modelling to develop a composition-property model for alkali-activated materials. Composites Part B: Engineering, Vol. 216, 2021, id. 108801.
- [25] Zhang, L. V., A. Marani, and M. L. Nehdi. Chemistry-informed machine learning prediction of compressive strength for alkaliactivated materials. Construction and Building Materials, Vol. 316, 2022, id. 126103.

- [26] Dao, D. V., H.-B. Ly, S. H. Trinh, T.-T. Le, and B. T. Pham. Artificial intelligence approaches for prediction of compressive strength of geopolymer concrete. Materials, Vol. 12, 2019, id. 983.
- Γ271 Nguyen, K. T., Q. D. Nguyen, T. A. Le, J. Shin, and K. Lee. Analyzing the compressive strength of green fly ash based geopolymer concrete using experiment and machine learning approaches. Construction and Building Materials, Vol. 247, 2020, id. 118581.
- Г281 Ramagiri, K. K., S. P. Boindala, M. Zaid, and A. Kar, Random forestbased algorithms for prediction of compressive strength of ambient-cured AAB concrete - A comparison study. In International Conference on Structural Engineering and Construction Management, 2021, pp. 717-725.
- [29] Toufigh, V. and A. Jafari. Developing a comprehensive prediction model for compressive strength of fly ash-based geopolymer concrete (FAGC). Construction and Building Materials, Vol. 277, 2021, id. 122241.
- [30] Peng, Y. and C. Unluer. Analyzing the mechanical performance of fly ash-based geopolymer concrete with different machine learning techniques. Construction and Building Materials, Vol. 316, 2022, id. 125785.
- Gomaa, E., T. Han, M. ElGawady, J. Huang, and A. Kumar. Machine learning to predict properties of fresh and hardened alkali-activated concrete. Cement and Concrete Composites, Vol. 115, 2021, id. 103863.
- [32] Gandomi, A. H. and D. A. Roke. Assessment of artificial neural network and genetic programming as predictive tools. Advances in Engineering Software, Vol. 88, 2015, pp. 63-72.
- Frank, I. E. and R. Todeschini. The data analysis handbook, Elsevier, [33] Amsterdam, The Netherlands, 1994.
- [34] Jin, C., Y. Qian, S. A. Khan, W. Ahmad, F. Althoey, B. S. Alotaibi, et al. Investigating the feasibility of genetic algorithms in predicting the properties of eco-friendly alkali-based concrete. Construction and Building Materials, Vol. 409, 2023, id. 134101.
- [35] Cao, Q., X. Yuan, M. Nasir Amin, W. Ahmad, F. Althoey, and F. Alsharari. A soft-computing-based modeling approach for predicting acid resistance of waste-derived cementitious composites. Construction and Building Materials, Vol. 407, 2023, id. 133540.
- Xia, X. Optimizing and hyper-tuning machine learning models for the water absorption of eggshell and glass-based cementitious composite. PloS one. Vol. 19, 2024, id. e0296494.
- [37] Lee, B. C. and D. M. Brooks. Accurate and efficient regression modeling for microarchitectural performance and power prediction. ACM SIGOPS operating systems review, Vol. 40, 2006, pp. 185-194.
- [38] Hadzima-Nyarko, M., E. K. Nyarko, H. Lu, and S. Zhu. Machine learning approaches for estimation of compressive strength of concrete. The European Physical Journal Plus, Vol. 135, 2020, id. 682.
- Huang, J., Y. Sun, and J. Zhang. Reduction of computational error by optimizing SVR kernel coefficients to simulate concrete compressive strength through the use of a human learning optimization algorithm. Engineering with Computers, Vol. 38, 2021, pp. 3151-3168.
- Ahmad, A., K. Chaiyasarn, F. Farooq, W. Ahmad, S. Suparp, and F. Aslam. Compressive strength prediction via gene expression programming (GEP) and artificial neural network (ANN) for concrete containing RCA. Buildings, Vol. 11, 2021, id. 324.
- [41] Farooq, F., W. Ahmed, A. Akbar, F. Aslam, and R. Alyousef. Predictive modeling for sustainable high-performance concrete from industrial wastes: A comparison and optimization of models using ensemble learners. Journal of Cleaner Production, Vol. 292, 2021, id. 126032.

18

- [42] Aslam, F., F. Farooq, M. N. Amin, K. Khan, A. Waheed, A. Akbar, et al. Applications of gene expression programming for estimating compressive strength of high-strength concrete. *Advances in Civil Engineering*, Vol. 2020, 2020, pp. 1–23.
- [43] Lundberg, S. M. and S.-I. Lee. A unified approach to interpreting model predictions. 31st Conference on Neural Information Processing Systems (NIPS 2017), Long Beach, CA, USA, Vol. 30, 2017.
- [44] Lundberg, S. M., G. G. Erion, and S. I. Lee. Consistent individualized feature attribution for tree ensembles. arXiv preprint arXiv:1802.03888, 2018.
- [45] Naqi, A. and J. G. Jang. Recent progress in green cement technology utilizing low-carbon emission fuels and raw materials: A review. Sustainability, Vol. 11, 2019, id. 537.
- [46] Valente, M., M. Sambucci, M. Chougan, and S. H. Ghaffar. Reducing the emission of climate-altering substances in cementitious materials: A comparison between alkali-activated materials and Portland cement-based composites incorporating recycled tire rubber. *Journal of Cleaner Production*, Vol. 333, 2022, id. 130013.
- [47] Luukkonen, T., Z. Abdollahnejad, J. Yliniemi, P. Kinnunen, and M. Illikainen. One-part alkali-activated materials: A review. *Cement and Concrete Research*, Vol. 103, 2018, pp. 21–34.
- [48] Khan, K., W. Ahmad, M. N. Amin, A. Ahmad, S. Nazar, and M. A. Al-Faiad. Assessment of artificial intelligence strategies to estimate the strength of geopolymer composites and influence of input parameters. *Polymers*, Vol. 14, 2022, id. 2509.